phys. stat. sol. (a) **122**, 723 (1990)

Subject classification: 73.40 and 85; S8.15

Fachbereich Physik der Humboldt-Universität zu Berlin, Institut für Optik und Spektroskopie[1])

Spatially Variable Drift Mobility Model for $Hg_{1-x}Cd_xTe$ Diodes

II. Application to Device Simulation[2])

By

A. SCHENK

A spatially variable drift mobility model for $Hg_{1-x}Cd_xTe$ with $x \approx 0.2$, outlined in a previous paper, is applied to infrared photodiodes. For this purpose the mobility program was self-consistently incorporated into the 2D device simulator TOSCA. Zero voltage mobility profiles of electrons and heavy holes are obtained restricting the scattering mechanisms to polar optical phonon and ionized impurity scattering for clearness. Besides the doping profile and the dominating scattering processes, the local mobility is determined by degeneracy and screening effects. Forward biased, heavily doped junctions exhibit a remarkable change of the mobility profile. The averaged mobility increases with rising positive voltage, which results in steeper I–U curves. The reverse biased mobility profile is only little affected, but reflects the increasing depletion by a broadening mobility well.

Ein ortsabhängiges Modell der Driftbeweglichkeit in $Hg_{1-x}Cd_xTe$ mit $x \approx 0{,}2$, das früher entwickelt wurde, wird auf Infrarot-Photodioden angewendet. Dazu wurde das Beweglichkeitsprogramm selbstkonsistent in den 2D-Bauelemente-Simulator TOSCA eingebaut. Man erhält Beweglichkeitsprofile der Elektronen und schweren Löcher im Gleichgewicht, wobei zur Deutlichkeit nur die Streuung an polar-optischen Phononen und ionisierten Störstellen berücksichtigt wurde. Neben dem Dotierungsprofil und den dominanten Streuprozessen wird die lokale Beweglichkeit von Entartungs- und Abschirmungseffekten bestimmt. Stark dotierte und positiv vorgespannte Übergänge zeigen eine beträchtliche Veränderung des Beweglichkeitsprofils. Die mittlere Beweglichkeit wächst mit steigender positiver Spannung, was zu steileren I–U-Kurven führt. Im Sperrfall wird das Beweglichkeitsprofil nur leicht verändert, es spiegelt jedoch direkt die wachsende Verarmung durch ein breiter werdendes Beweglichkeitsminimum wieder.

1. Introduction

The theoretical background of a spatially variable drift mobility model in $Hg_{1-x}Cd_xTe$ with $x \approx 0.2$ has been outlined in a previous paper [1], hereafter denoted I. Using the Kohler variational method, all relevant scattering mechanisms in $Hg_{0.8}Cd_{0.2}Te$ were included. The particular situation in HgCdTe devices with degeneracy, alloy scattering, implantation related structural defects, and different kinds of impurities was reflected. Furthermore, the model has been compared with experimental Hall data to select the proper microscopic parameters. Owing to the analytical simplicity of the model the numerical expense could be restricted to a level necessary for application in device simulation packages.

As a first result, electron and heavy hole mobility profiles in a 1D model of real infrared detector diodes were calculated solving the neutrality equation. Both mobilities varied over one order of magnitude, which gave rise to expect remarkable effects in device simulation. These effects are investigated in more detail in the present paper.

---

[1]) Invalidenstr. 110, O-1040 Berlin, FRG.

[2]) Part I see phys. stat. sol. (a) **122**, 413 (1990).

In Section 2 the integration of the mobility routine into the 2D device simulator TOSCA is briefly described. Numerical results of mobility profiles for different bias conditions will be discussed in Section 3. Section 4 demonstrates, how different mobility models affect the I–U characteristics. A brief conclusion is presented in Section 5.

2. Integration into the 2D Device Simulator TOSCA

The 2D device simulator TOSCA [2] solves the van Roosbroeck system of semiconductor device equations by the method of finite elements [3 to 5]. Besides the electronic problem certain components of the coupled optical problem are included, e.g. optical wave guiding and optical generation of carriers. This enables TOSCA to simulate a broad class of electronic and optoelectronic devices, such as MOSFETs, MESFETs, photodiodes, CCDs, LEDs, and diode lasers. Furthermore, TOSCA serves as an experimental tool to test new quantum-mechanical models, as it has been done in the case of interband tunneling [6, 7] to simulate the soft breakdown in HgCdTe photodiodes.

The mobility model outlined in I has been incorporated into TOSCA for alternative use besides some simpler standard models. Scattering mechanisms and microscopic parameters reflect the particular situation in $Hg_{1-x}Cd_xTe$ with $x \approx 0.2$. Since polar optical phonon (po) and ionized impurity scattering (cc) are the most relevant ones at the infrared sensor operation temperature $T = 77$ K, the model becomes applicable to other materials if the set of microscopic parameters is changed. The remaining scattering processes considered include neutral impurity scattering (nc), alloy scattering (dis), strain field scattering (sf), piezoelectric (pz), and acoustic phonon scattering (ac).

The spatial variability of the mobility is not only a direct consequence of the ionized (and neutral) impurity distribution in the device. It has a second origin in the dependence on the density of free carriers, if they are degenerate. Then, the mobility is a function of the quasi-Fermi level, and screening of the Coulombic interactions plays an important role. Therefore, one is faced with a self-consistent problem, because the variables of the van Roosbroeck system, the electrostatic potential $\varphi(\boldsymbol{r})$ and the carrier densities $n(\boldsymbol{r})$, $p(\boldsymbol{r})$ (or the quasi Fermi levels $F_n(\boldsymbol{r})$, $F_p(\boldsymbol{r})$, respectively), enter the mobility.

The carrier densities and the quasi-Fermi levels, determined at each grid point with Fermi statistics and Kane band structure, are passed on by the main program to the mobility routine. The electron and heavy hole mobilities then are calculated for all grid points and enter the current matrix equations. How the electron mobility changes with applied voltage, will be described in the next section.

It was pointed out in I that one numerical integration within the mobility program is necessary to treat degeneracy effects correctly. Therefore, the CPU time increases remarkably, by a factor 10 to 20, compared with the case of constant mobilities and depending on the number of vertices.

3. Mobility Profiles for Different Bias Conditions

Since we are not interested in lateral effects here, but in the essential influence of the spatially variable mobility model on device operation, we limit ourselves to a narrow, quasi-one-dimensional domain. Its size is 0.3×11 μm^2, and it involves 213 vertices. The doping profile is assumed to vary in y-direction only, and all illustrations will be section drawings along this direction.

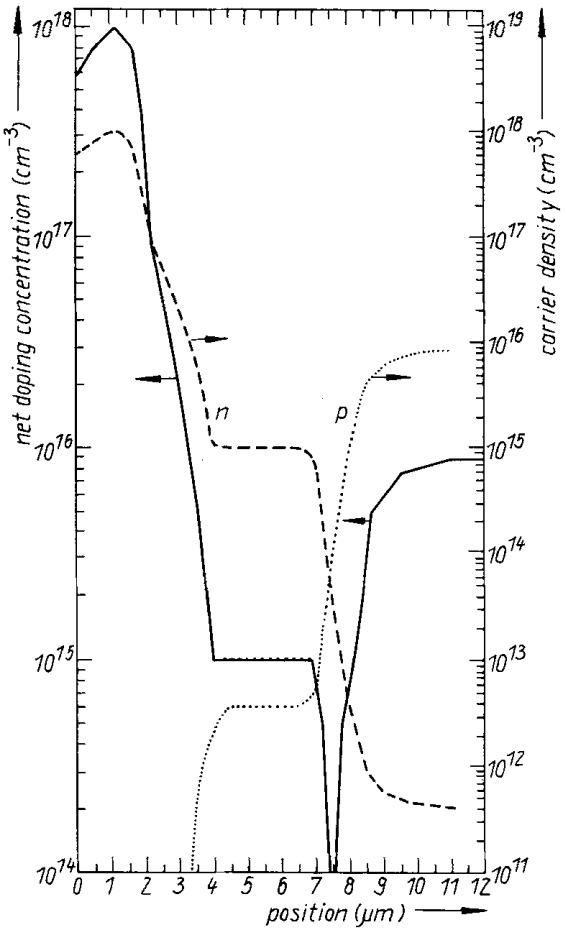

Fig. 1. Net doping profile of the assumed, completely ionized, residual impurities of the n^+n^-p junction (———) and the corresponding free carrier densities

First, we demonstrate the spatial variability of the mobility in $Hg_{0.8}Cd_{0.2}Te$ at zero voltage for a n^+n^-p junction profile. The concentration of completely ionized residual impurities and the free carrier densities are shown in Fig. 1. The set of mobility parameters has been chosen such that po scattering and cc scattering dominate (nc and sf scattering are suppressed). The resulting mobility profiles for electrons and heavy holes are shown in Fig. 2. As outlined in I, the electron mobility of the n^+n^-p junction at 77 K is determined by cc scattering over the whole structure.

The explanation of the profile is as follows: In the n^+-region the electron gas is highly degenerate. Therefore, despite the large impurity concentration, the mobility is comparatively high (2.7×10^5 cm^2/Vs) and spatially constant. It decreases to a level of about 6×10^4 cm^2/Vs within the n^+n^- transition region, since screening becomes less efficient. The minimum is reached in the depletion layer. In the p-region both kinds of carriers are nondegenerate, and the electron mobility follows the decrease in total impurity concentration, reaching a maximum of 3.4×10^5 cm^2/Vs at the p-contact.

In the case of heavy holes the cc scattering dominates only in the n^+-region. The hole mobility reflects directly the impurity profile there (minimum 58 cm^2/Vs). The po scattering is the most important one in the n^-p region, resulting in an almost constant mobility of 450 to 500 cm^2/Vs.

Obviously, besides the impurity profile and possible changes of the dominating scattering mechanism, degeneracy and screening, both connected with larger carrier concentrations, determine the mobility at a certain position in the device. Therefore, one expects a modification of the mobility profiles, if an external voltage is applied. This is demonstrated in Fig. 3a for the case of the electron mobility in the n^+n^-p structure (cf. Fig. 2). A forward bias injects electrons into the n^--region, where they become more and more degenerate. Fig. 3b shows the corresponding electron concentration in the n^+n^- region. The mobility increases with rising voltage. At $U = 0.1$ V its value in the n^--region becomes larger than the unchanged one in the n^+-region, due to the lower impurity concentration. A new maximum emerges distinctly in the p-region, where degeneracy effects come into play at

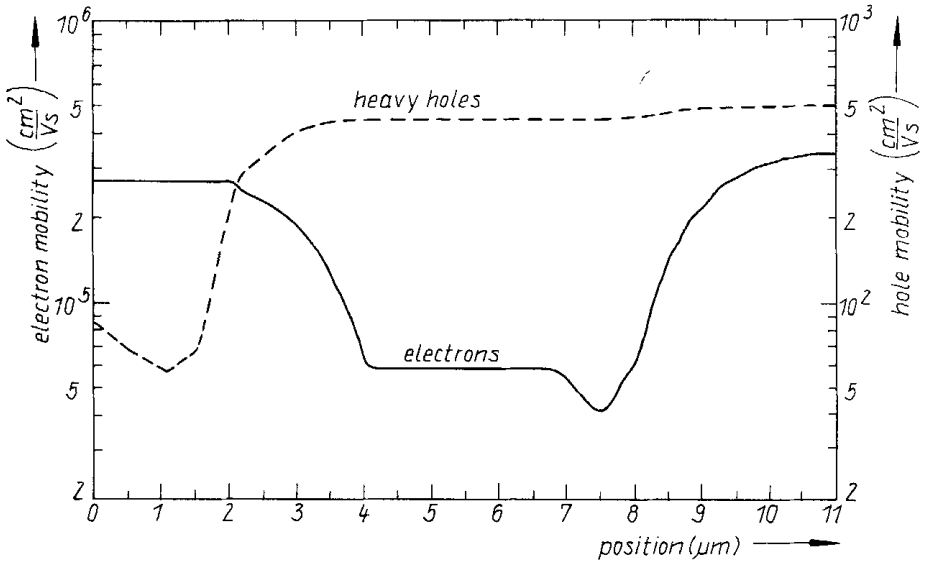

Fig. 2. Electron and heavy hole mobility profiles of the n^+n^-p junction. Only po and cc scattering were taken into account. The microscopic parameters are listed in I [1]

higher biases, but at the same time the Fermi level remains pinned on the p-side boundary, since the p-contact was taken as ideal Ohmic. The steep gradient on the p-side Ohmic contact originates from the shortness of the investigated structure (11 μm).

Altogether, the averaged electron mobility of the n^+n^-p structure increases with rising positive voltage, which strengthens the current density additionally.

The increase in the local conductivity, shown in Fig. 3c for the n^+n^- region, is much more pronounced than the increase in the mobility alone.

The mobility profile of the reverse biased diode (Fig. 3a) is changing only in the depletion region. It decreases slightly there. The progressive depletion is directly reflected by a broadening mobility well.

The main result of this section is that the mobility depends on applied voltage in a complex way as soon as the junction contains a degenerate region.

4. *I–U* Characteristics

As pointed out in the previous section, the electron mobility of a n^+n^-p $Hg_{0.8}Cd_{0.2}Te$ photodiode is a nonlinear function of the forward bias. Thus, one expects that *I–U* curves derived from constant mobilities are bent, if the spatially variable model is used. This is clearly seen from Fig. 4a. No constant averaged mobility value can reproduce the correct *I–U* characteristic over the whole positive voltage axis. Only $\mu_n = 2 \times 10^5$ cm^2/Vs gives accordance from $U = 20$ to 50 mV. At higher biases a strong deviation from the presented model occurs.

The corresponding small bias curves (−10 to 10 mV) are shown in Fig. 4b. Here, it is possible to verify the correct differential resistance at zero voltage with a constant electron mobility of 2.4×10^5 cm^2/Vs. It can be concluded from the above results that due to injection of majority carriers the increasing mobility of the minority carriers, which determine the device operation, can remarkably change the *I–U* characteristic.

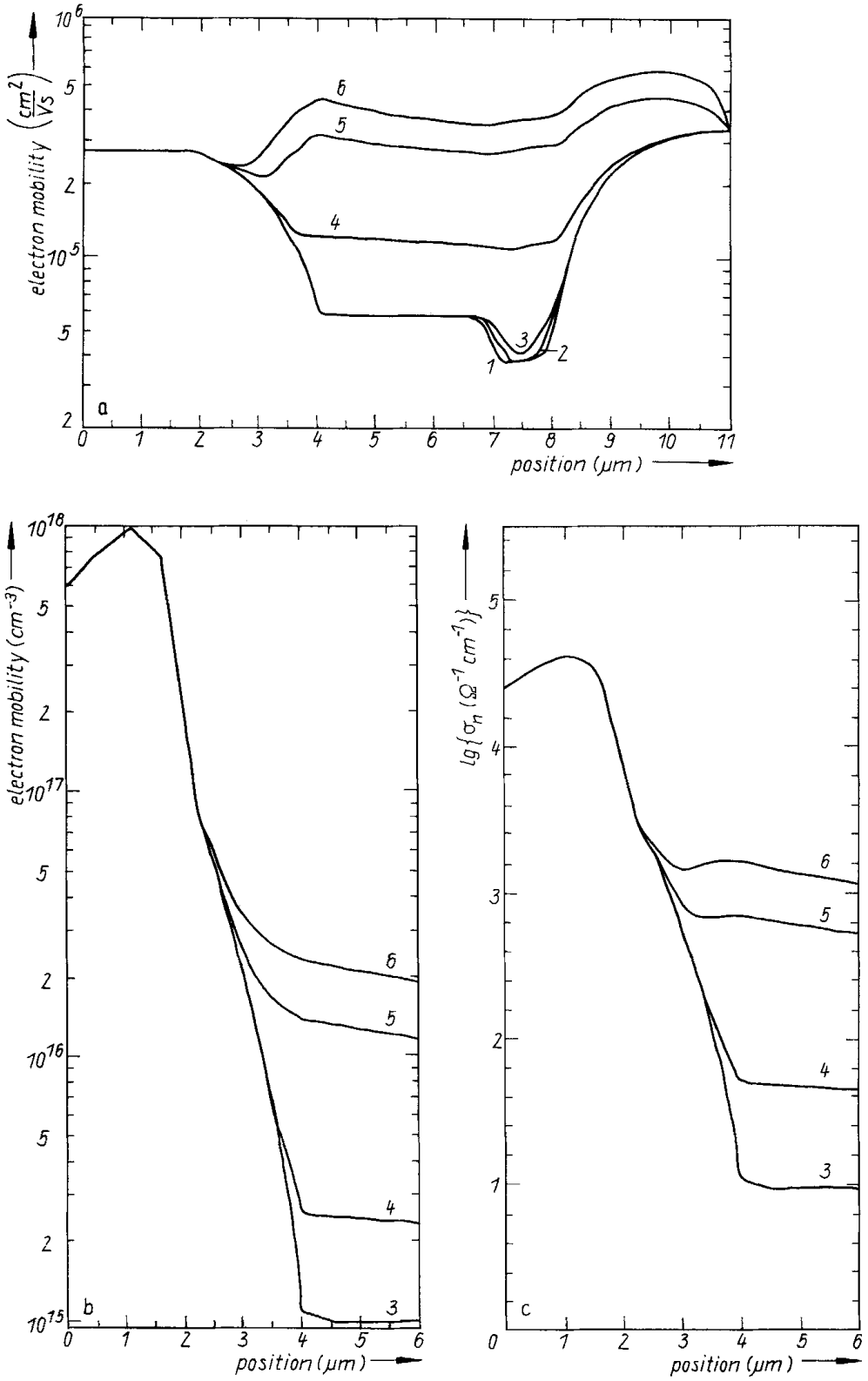

Fig. 3.a) Electron mobility of the n^+n^-p junction for different applied voltages: (1) −200 mV, (2) −100 mV, (3) 0 V, (4) +50 mV, (5) +100 mV, (6) +150 mV. Parameters listed in I [1]. b) Electron concentration of the n^+n^-p junction in the n^+n^- region for the same forward biases. c) Electron conductivity profiles of the n^+n^-p junction in the n^+n^- region for the same forward biases

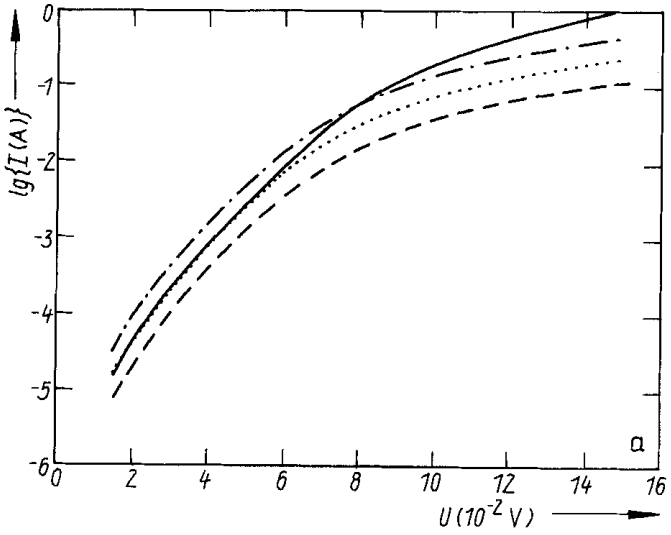

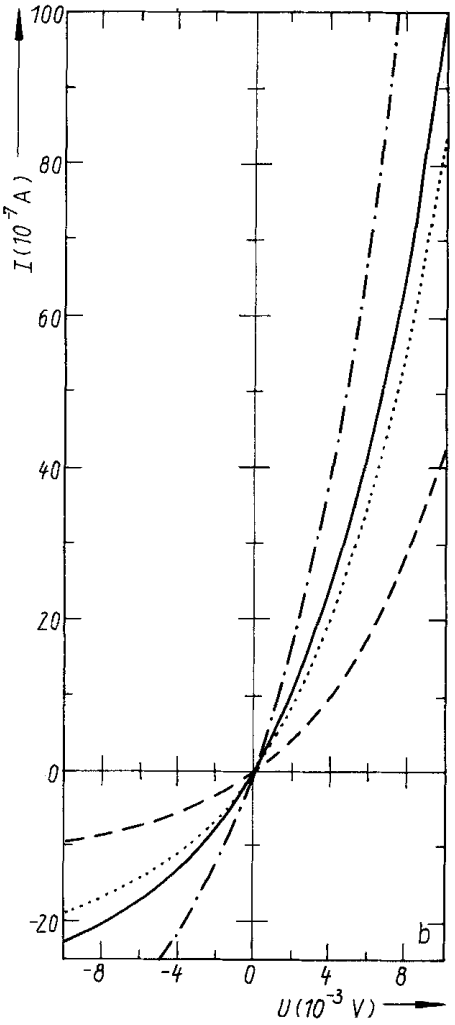

Fig. 4. Comparison of the I–U characteristics of the n^+n^-p junction with spatially variable model (———) and with constant electron mobilities: 1×10^5 cm^2/Vs (– – –), 2×10^5 cm^2/Vs (· · · · · ·), 4×10^5 cm^2/Vs (— · — · —). The constant heavy hole mobility is $\mu_{hh} = 300$ cm^2/Vs

5. Conclusions

In this paper a spatially variable drift mobility model for $Hg_{0.8}Cd_{0.2}Te$ photodiodes, developed in I [1], has been investigated numerically. It was incorporated into the 2D device simulator TOSCA [2], which serves for modelling optoelectronic devices by the method of finite elements. The electron and heavy hole mobilities are evaluated self-consistently in every Gummel step at all grid points in the program. Specializing the structure to a quasi-one-dimensional domain, zero-voltage mobility profiles were calculated for a n^+n^-p junction. The variety of possible scattering mechanisms was reduced to po and cc scattering for clearness. The local mobility is determined by the doping profile, by the dominating scattering mechanisms, and by degeneracy and screening effects. Since the mobility depends on the carrier density, except if Boltzmann statistics holds utterly, its profile may change with applied voltage. This leads to an increasing averaged mobility in the case of majority carrier injection. $I-U$ curves become steeper than they would be using a constant mobility value. This feature was demonstrated for a n^+n^-p junction in $Hg_{1-x}Cd_xTe$. The reverse biased $I-U$ curve is only little affected, but the rising depletion layer is directly reflected by a broadening mobility well.

The described effect should apply to all heavily doped junctions and to junctions, where a change from Boltzmann to Fermi statistics occurs during operation. The program, properly modified for application to such junctions in other materials, should be especially helpful for devices with forward bias operation, like diode lasers.

Acknowledgement

The author is indebted to Prof. H. Gajewski from Karl-Weierstrass-Institute of Mathematics (Academy of Sciences) for implementing the mobility routine into the 2D device simulator TOSCA. His unceasing interest and many discussions are gratefully acknowledged.

References

[1] A. SCHENK, phys. stat. sol. (a) **122**, 413 (1990).
[2] H. GAJEWSKI, TOSCA-Handbook, Berlin 1989.
[3] W. VAN ROOSBROECK, Bell Syst. tech. J. **29**, 560 (1950).
[4] S. SELBERHERR, Analysis and Simulation of Semiconductor Devices, Springer-Verlag, 1984 (p. 181).
[5] P. A. MARKOWICH, The Stationary Semiconductor Device Equations, Springer-Verlag, 1985 (p. 133).
[6] A. SCHENK, M. STAHL, and H.-J. WÜNSCHE, phys. stat. sol. (b) **154**, 815 (1989).
[7] M. STAHL, to be published.

(Received June 14, 1990; in revised form September 6, 1990)